Journal of Drug Targeting

http://informahealthcare.com/drt
ISSN: 1061-186X (print), 1029-2330 (electronic)

J Drug Target, Early Online: 1–13
 DOI: 10.3109/1061186X.2015.1052075

informa
healthcare

ORIGINAL ARTICLE

Inhibitory effect of epirubicin-loaded lipid microbubbles with conjugated anti-ABCG2 antibody combined with therapeutic ultrasound on multiple myeloma cancer stem cells

Fangfang Shi[1,2]*, Fang Yang[3]*, Xiangfeng He[4]*, Ying Zhang[1], Songyan Wu[1], Miao Li[1], Yunxia Zhang[1,2], Wu Di[1], Jun Dou[1], and Ning Gu[3]

[1]*Department of Pathogenic Biology and Immunology, School of Medicine & Collaborative Innovation Center of Suzhou NanoScience and Technology, Southeast University, Nanjing, China,* [2]*Department of Oncology, Zhongda Hospital, School of Medicine, Southeast University, Nanjing, China,* [3]*School of Biological Science & Medical Engineering & Collaborative Innovation Center of Suzhou NanoScience and Technology, Southeast University, Nanjing, China, and* [4]*Department of Medical Oncology, Affiliated Tumor Hospital of Nantong University, Nantong, China*

Abstract

Ultrasound-targeted microbubble destruction (UTMD) technique is thought to improve the chemotherapeutic agent delivery from microbubbles (MBs) in tumor tissues and reduce the side effects in non-tumor tissues. Multiple myeloma (MM) is a bone marrow cancer and remains to be an incurable disease. In this study, we used the UTMD technique to investigate the inhibitory effect of our developed novel reagent on MM cancer stem cells ($CD138^-CD34^-$MM CSCs) that are MM cells with $CD138^-CD34^-$ phenotypes, responsible for MM-initiating potential, drug resistance and eventual relapse. The preparatory steps of novel reagent was first epirubicin (EPI)-loaded in the lipid MBs that was consisted of 1,2-distearoyl-sn-glycero-3-phosphoethanolamine-*N*-[methoxy(polyethylene glycol)-2000]-biotin, dipalmitoyl-phosphatidylglycerol and 25-NBD-cholesterol, then anti-ABCG2 monoclonal antibody (mAb) was conjugated onto the MB surface to form EPI-MBs+mAb. $CD138^-CD34^-$MM CSCs were isolated from human MM RPMI 8226 cell line by the magnetic associated cell sorting method. The results showed that the attenuated proliferation, migration and invasion ability, and increased apoptosis were observed when MM CSCs were incubated with a various agents. EPI-MBs+mAb combined with therapeutic ultrasound significantly promoted the MM CSC apoptosis compared with EPI, EPI-MBs alone or EPI-MBs+mAb without ultrasound exposure. These results suggest that the developed EPI-MBs+mAb combined with therapeutic ultrasound remarkably induced MM CSC apoptosis *in vitro*.

Keywords

ATP-binding cassette sub-family G member 2 (ABCG2), cancer stem cells, conjugation, epirubicin, microbubble, multiple myeloma

History

Received 26 March 2015
Revised 5 May 2015
Accepted 13 May 2015
Published online 23 July 2015

Introduction

Multiple myeloma (MM) is a bone marrow cancer characterized by the neoplastic proliferation of a plasma cell clone and production of monoclonal immunoglobulin. Patients with MM usually clinically result in lytic bone lesions, hypercalcemia, anemia, immunodeficiency and renal insufficiency [1,2]. MM accounts for approximately 10% of hematologic cancers [2,3].

Based on the investigation on the biology of MM and the bone-marrow microenvironment, autologous stem-cell transplantation and new chemotherapeutic agents including thalidomide, lenalidomide and bortezomib were introduced in the past decade, causing not only improved chemotherapeutic complete response rates but also prolonged the median survival greatly in MM patients [4]. However, nearly all patients with MM eventually become refractory to these therapies. Consequently, the outcome of MM patients is very poor [5,6]. The failure of therapy is thought to be associated with a persistent sub-population of tumor cells that are named MM cancer stem cells (MM CSCs) or myeloma initiating cells. MM CSCs are probably both resistant to anti-MM chemotherapy and having the growth potential to mediate disease relapse [7–10]. Therefore, development of targeted delivery of drugs to MM CSCs should have a profound impact on MM eradication.

Microbubbles (MBs) are small gas bubbles with the diameter from 1 to 10 μm, stabilized by a lipid, polymer or protein shell and have undergone a rapid development for use as a drug delivery system [11,12]. Nano-scale MBs usually have the diameter within 1 μm. Under a certain acoustical

*These authors contributed equally to this work.

Address for correspondence: Dr. Jun Dou, Department of Pathogenic Biology and Immunology, School of Medicine & Collaborative Innovation Center of Suzhou NanoScience and Technology, Southeast University, 87# Ding Jiaqiao Rd., Nanjing 210009, China. Tel: +86 25 83272454. E-mail: njdoujun@seu.edu.cn
Dr. Ning Gu, School of Biological Science & Medical Engineering & Collaborative Innovation Center of Suzhou NanoScience and Technology, Southeast University, 2# Sipai Lou, Nanjing 210096, China. Tel: +86 25 83272326. E-mail: guning@seu.edu.cn

condition, MBs physically interact with some target tissues and increase temporarily the drug uptake by cells with improved cell permeability [12–14]. Nevertheless, MB release of drugs and the drug uptake by cells hardly appear in tissues without ultrasound exposure. Thus, the ultrasound-targeted microbubble destruction (UTMD) technique is thought to improve the chemotherapeutic agent delivery from MBs in tumor tissues and reduce the side effects in non-tumor tissues. It is known that the ability of MBs to scatter ultrasound so effectively is largely due to their compressibility. This can best be understood by considering the pressure balance at the surface of a spherical gas bubble suspended in an infinite volume of liquid. The volume of MBs can easily change due to the high compressibility of the gas inside. Thus, when exposed to an ultrasound field, the MBs will undergo volumetric oscillations in response to the varying pressure [15]. Consequently, using UTMD technique in cancer treatment to increase the efficiency of chemotherapy through passive, localized delivery has been an emerging area of research [14–16].

Epirubicin (EPI) is one of the anthracyclines used in the treatment of MM, breast cancer, osteosarcomas, aggressive lymphomas, etc. EPI makes DNA intercalation, lipid peroxidation and inhibition of topoisomerase II. EPI-loaded MBs combined with therapeutic ultrasound are expected to improve the EPI release and uptake in ultrasound-treated tumors and reduce the adverse effects of EPI, especially the dose-dependent cardiotoxicity [11,17].

Accumulating evidence indicates that MM CSCs usually up-regulate expression of ATP-binding cassette (ABC) transporters including efflux drug pumps of ABCB1, ABCC1 and ABCG2 that is related to drug resistance [18]. This is because ABCG2 transporter enables a cancer to be not affected by the cytotoxic effect of chemotherapy that kills most cells in a tumor. Thus, blocking the chemotherapeutic drug efflux from the tumor cells may be a good strategy for generation of continuous cytotoxic effect on MM CSCs [19]. For this reason, we developed a EPI-loaded MBs with conjugated anti-ABCG2 monoclonal antibody (EPI-MBs+mAb) that could directly target the ABCG2 molecule overexpressed on the surface of MM CSCs, and used a novel agent combined with UTMD to investigate the inhibitory effect on MM CSCs as marked $CD138^{-}CD34^{-}$ phenotypes by isolated from human MM RPMI 8226 cell line *in vitro*. Our results indicate that the combination of EPI-MBs+mAb with therapeutic ultrasound exhibited significant inhibition of $CD138^{-}CD34^{-}$MM CSC growth, induced obvious apoptosis and overcame the cell resistant to EPI. This study therefore suggests a potential anti-cancer regimen that is worth of further investigation on treatment of MM CSCs *in vivo*.

Materials and methods

Cell culture

Human MM RPMI 8226 cell line was purchased from the Cell Institute in Beijing, People's Republic of China. Cells were cultured in complete medium consisting of RPMI 1640, 2 mM L-glutamine, 100 U/mL penicillin, 100 μg/mL streptomycin and 10% fetal bovine serum at 37 °C in a humidified incubator containing 5% CO_2.

Main materials

EPI was purchased from Dalian Meilun Biotech CO., Ltd. of China. 3-(4,5-Dimethyl-2-thiazyl)-2,5-diphenyl-2H-tetrazoliumbro-mide (MTT) and trypan blue were purchased from Sigma Corporation (St. Louis, Mo, CA). Mouse antihuman CD138 and CD34 mAb labeled microbeads were purchased from Miltenyi Company (Gladbach, Germany). Matrigel was purchased from BD Biosciences (San Jose, CA). The annexin V-PE/7-AAD apoptosis assay kit (KGA1017) and cell counting kit-8 (CCK-8) were purchased from Nanjing KeyGen Biotech. Co., Ltd (Nanjing, China). Anti-ABCG2 mAb was purchased from Cell Signaling Corporation (Danvers, MA). 1,2-Distearoyl-sn-glycero-3-phosphoethanolamine-*N*-[methoxy (polyethylene glycol)-2000]-biotin (DSPE-PEG 2000-Biotin), dipalmitoyl-phosphatidylglycerol (DPPG) and 25-NBD-cholesterol were purchased from Avanti Polar Lipids, Inc. (Alabaster, Al). Perfluoropropane (C_3F_8) was purchased from Nuclear Industry Institute of Physical and Chemical Engineering (Shanghai, China). Streptavidin, FITC-streptavidin and FITC-labeled goat anti-mouse IgG were purchased from Sigma-Aldrich, Inc. (St. Louis, Mo, CA). All other chemicals were commercially available and of analytical grade.

Preparation of EPI-MBs

DPPG/DSPE-PEG2000-Biotin/25-NBD-cholesterol (90:5:5, molar ratio) dissolved in chloroform was added to the round bottom flask. Chloroform was then removed with vacuum evaporation until a thin film was observed. Highly purified electrolyte-free water with EPI (0.5 mg/ml), EDTA (0.003 mg/ml) and glucose (50 mg/ml) was added to the dried lipids thin films (lipid concentration of 1 mg/ml) [20,21]. The lipid suspension was then mixed well at the phase transition temperature of the lipids (60 °C) to form a milky solution of multilamellar liposomes. Then the multilamellar liposomes suspension was continuously sonicated at 100 W with an ultrasonic cell disruptor (Branson Ultrasonics Corporation, Danbury, CT) with a constant purging of C_3F_8 gas (4 ml/min) for 5 min to form the EPI-loaded lipid biotinylated MBs. The freshly prepared MBs were kept in 4 °C for 1 h to stratify. Then, MBs with larger diameters in the top white foam layer were discarded. The milky suspension in the lower layer was collected and washed with PBS three times (1500 rpm, 3 min) to remove free EPI and liposomes [22–25].

Preparation of EPI-MBs+mAb

The biotinylated EPI-MBs stock solution was pipetted into an EP tube and diluted $5–6 \times 10^8$ with PBS. Streptavidin was added at 0.04 mg/ml to the diluted MB solution, mixed well and incubated for 15 min at room temperature with gentle shaking. After reaction, the MB solution was washed (1500 rpm, 3 min) three times to remove the excess avidin. Avidinylated EPI-MBs were obtained. Anti-ABCG2 mAb was biotinylated by sulfo-NHS-LC-biotinylation kit (Thermo Scientific, Inc., Waltham, MA). Biotinylated anti-ABCG2 mAb was then added into streptavidin-treated MBs and mixed in a ratio of 10^8 EPI-MBs to 20 μg anti-ABCG2 mAb. The mixtures were left at 4–8 °C for 1 h for incubation with gentle shaking. MBs carrying anti-ABCG2 mAb were washed three

times to remove free antibody [17,25]. In the trial confirming streptavidin on the surface of EPI-MBs+mAb, FITC-streptavidin was used instead of streptavidin.

Characterization of EPI-MBs+mAb

The morphology of EPI-MBs and EPI-MBs+mAb was observed by using optical microscopy and confocal laser scanning microscope (Olympus, Tokyo, Japan). The mean size, size distribution and zeta potential of MBs were measured with a Malvern Zetasizer Nano ZS unit (Malvern Instrument, Malvern, UK) [25]. EPI encapsulation efficiency was determined in triplicate using ultraviolet–visible (UV–Vis) spectrophotometry (Metash Instruments Co., Shanghai, China) by determining the amount of EPI recovered from washed supernatants during preparation (free EPI) at an excitation wavelength, $\lambda_{ex} = 233$ nm. Drug payload was calculated as the difference between the total EPI and free EPI. EPI encapsulation efficiency was then calculated using the following equations [26]

$$\text{Encapsulation efficiency } (\%) = (\text{total EPI} - \text{free EPI})/\text{total EPI} \times 100\%$$

Detection of anti-ABCG2 mAb on the surface of EPI-MBs+mAb

A total volume of 5 ml (5×10^8) biotinylated EPI-MBs or EPI-MBs+mAb was mixed with 1 ml FITC-labeled goat anti-mouse IgG and the solution was allowed to react in the dark in a 37 °C incubator for 1 h followed by centrifugation at 1500 rpm for 3 min and washed with PBS for three times to remove excess goat anti-mouse IgG. Binding of the secondary antibody with biotinylated EPI-MBs and EPI-MBs+mAb was observed by confocal fluorescence microscope [25]. The conjugation efficiency of anti-ABCG2 mAb on the surface of EPI-MBs+mAb was detected according to fluorescent intensity of FITC-conjugated secondary antibody by FCM (Beckman Coulter, Brea, CA) [17].

Isolation of MM $CD138^-CD34^-$ cells

$CD138^-CD34^-$ cells were isolated from the human MM RPMI 8226 cell line by a magnetic activated cell sorting method (Miltenyi Biotec, Gladbach, Germany) following our previous study [27]. We named $CD138^-CD34^-$ cells for MM CSCs. This was accomplished through our previous analysis of the characteristics of $CD138^-CD34^-$ cells that share the CSC characteristics [27,28].

Proliferative and clonal assays of MM $CD138^-CD34^-$ cells

2×10^3 $CD138^-CD34^-$ or non-$CD138^-CD34^-$ cell suspensions were seeded into 96-well plates and were assayed for proliferative activity in triplicate wells. To test for cell viability, the cell suspensions were mixed with 0.4% Trypan blue (Sigma, St. Louis, Mo, CA) after 1, 2, 3, 4, 5 and 6 days of incubation; mean values of the viable counts was obtained by a hemocytometer chamber [28].

The colony-forming assay in the soft agar medium was performed by following our previous method [28]. Colony efficiency was determined as the number of colonies formed divided by the total number of cells planted [29]. As control, non-$CD138^-CD34^-$cells were used in the assay.

Some cells in complete medium containing EPI-MBs or EPI-MBs+mAb were carried out with exposure to ultrasound or without exposure to ultrasound. This special explanation is also used in the assays below.

Drug resistance assay

4×10^3 $CD138^-CD34^-$ and non-$CD138^-CD34^-$ cell suspensions were, respectively, seeded into a 96-well plate at 37 °C in 5% CO_2. EPI was administered at a dose of 10 μg/ml. Each well was added with 200 μl cells for 24 h, and cells were washed in PBS for three times, and then 20 μL of Cell Counting Kit-8 (CCK8) solution was added to each well for additional 1.5 h of culture. The absorbance at 490 nm was recorded using a microplate reader (Model 550, Bio-Rad, Hercules, CA) [27]. The resistant rate to EPI of $CD138^-CD34^-$ and non-$CD138^-CD34^-$ cells was respectively calculated.

Migration and invasion assays

2×10^5 $CD138^-CD34^-$ or non-$CD138^-CD34^-$ cells were resuspended in complete medium and seeded into the upper compartments of polycarbonate Transwell® two-chamber migration plates (Costar®, Corning Inc, Corning, NY). The assays were performed by following the method as was described previously [27,30]. The ultrasound protocol and the transducer type are described below.

Effect of ultrasound on $CD138^-CD34^-$ cells

Ultrasound exposure system is the same as described previously [24]. An arbitrary waveform generator (Agilent 33250A, Agilent Technologies Inc., Palo Alto, CA) was used to produce a sinusoidal radio frequency signal; it contained repeated 1 MHz tone-bursts and 20 cycles per tone-burst at a pulse repetition frequency of 10 kHz. It was then amplified by a 50 dB broadband repetition frequency power amplifier (ENI 2100L, Rochester, NY), and used to drive a selfmade focusing transducer of radius 9.2 cm. The central frequency of the transducer is 1 MHz and the focal distance was 8 cm. The plastic test tube of 15 mm diameter and 75 mm length (Kimble, Owens-Illinois, Toledo, OH) filled with cells capped by a rubber stopper, which was used as an sound absorber to minimize a standing-wave effect and there was no air between the cap and suspension, was rotated at 60 rpm by a direct current motor throughout the exposure period and the rotation helped to mix MBs with cells evenly. 1×10^6 $CD138^-CD34^-$ cells were placed in the plastic tube, and were divided into control group (PBS only) and US group (ultrasound exposure only). Ultrasound pulses with an average intensity of 0.5 W/cm^2 were applied to the medium for 40 s in the US group. Then, the analyses of cell viability assay, apoptosis assay and transmission electron microscopy were applied as described below.

Ultrasound-mediated delivery of EPI

1×10^6 $CD138^-CD34^-$ cells were seeded in each tube, and a total of seven tubes were divided into a various treatment

groups: (a) PBS only (negative control); (b) EPI only; (c) EPI followed by ultrasound exposure (EPI+US); (d) EPI-MBs only; (e) EPI-MBs followed by ultrasound exposure (EPI-MBs+US); (f) EPI-MBs+mAb only and (g) EPI-MBs+mAb followed by ultrasound exposure (EPI-MBs+mAb+US) [17]. EPI was administered at a dose of 10 μg/ml in the other groups except the control group. Ultrasound pulses with the intensity of 0.5W/cm^2 and 40 se were applied in group EPI+US, EPI-MBs+US and EPI-MBs+mAb+US after the cells were incubated with the different agents 30 min.

EPI-MBs+mAb bind to MM CSCs

The specific bind of EPI-MBs+mAb to MM CSCs was determined with optical microscopy and FCM. 2×10^5 MM CD138$^-$CD34$^-$CSCs were incubated with PBS, EPI-MBs+mAb (1×10^8/ml) and EPI-MBs (1×10^8/ml) for 1 h respectively, and the cell clusters were placed upside down to maximize the cell–MBs interaction. Then cells were collected and washed with PBS three times to remove unbound EPI-MBs+mAb. The EPI-MBs+mAb bound to the MM CSCs were observed by a bright field microscope. All the experiments were carried out in triplicate.

Measurement of EPI accumulation in MM CSCs using FCM

Intracellular EPI fluorescence was measured by following the protocol previously described [31]. MM CSCs incubated, respectively, with PBS, EPI, EPI-MBs and EPI-MBs+mAb were treated as described in ultrasound-mediated delivery of EPI assay. Fifteen minutes after ultrasound pulses, cells were washed for three times with PBS and were analyzed by using a FCM (Beckman Coulter, Brea, CA) equipped with an argon ion laser and operated at 488 nm [32]. At least, 10 000 cells were analyzed in each sample. Within each experiment, determinations were performed in triplicate.

Cell viability assay

4×10^3 CD138$^-$CD34$^-$ cells were seeded in a 96-well plate and were incubated with the various chemotherapeutic agents, and exposure to ultrasound pulses for 24, 48 and 72 h, respectively. Then, cells were washed in PBS for three times and 20 μl of CCK8 solution was added to each well for additional 1.5 h of culture. The absorbance at 490 nm was recorded using a micro-plate reader (Model 550, Bio-Rad, Hercules, CA) [33].

Apoptosis assay

5×10^5 CD138$^-$CD34$^-$ cells were seeded into a 6-well plate in the presence of various chemotherapeutic agents, 24 h after exposure to ultrasound pulses. Cells were resuspended in binding buffer. Hundred microliters of cell suspension were incubated with Annexin V-PE and 7-AAD for 15 min at room temperature in the dark. The rate of apoptosis was analyzed by FCM (Beckman Coulter, Brea, CA) [34,35].

Transmission electron microscopy analysis

The ultrastructural morphology of untreated and treated MM CSCs was investigated by transmission electron microscopy (TEM, JEOL, Tokyo, Japan) by following the protocol previously described. Ultrathin sections were cut and placed on formvar-coated slot copper grids. Section were then counter stained with uranyl acetate and lead citrate and viewed with TEM [36].

Western blot analysis

1×10^6 CD138$^-$CD34$^-$ or non-CD138$^-$CD34$^-$ cells were collected and lyzed in the protein extraction buffer (Novagen, Madison, WI) by following the manufacturer's protocol. The rabbit antibody specific to human ABCG2 antibody (Santa Cruz Biotechnology, Dallas, TX) or rabbit antihuman caspase-8, caspase-9, caspase-3 or cleaved caspase-8, caspase-9, caspase-3 and GADPH (Bioworld, Louis Park, MN) were used in the assay [37,38].

Statistical analysis

The SPSS 19.0 software package (SPSS Corp., Chicago, IL) was used for data analysis. Data are expressed in the mean and standard deviations. The Student–Newman–Keuls test and one-way ANOVA were used to compare the variables among different groups. $p < 0.05$ was considered as statistically significant.

Results

Characterization of EPI-MBs and EPI-MBs+mAb

EPI was loaded to the MB shell through its high affinity to anionic phospholipids, such as phosphatidic acid, phosphatidylglycerol and cardiolipin. At physiological condition the EPI molecule bears one positive charge and possesses an amphiphilic character. Therefore, it can form non-covalent complexes with anionic phospholipids, stabilized mostly by electrostatic attractions and hydrophobic forces [20,21].

Figure 1(A) indicates images of MBs, EPI-loaded MBs (EPI-MBs) and EPI-MBs+mAb observed under an optical microscope. The EPI-MBs+mAb solution appears a good dispersity, and these different MBs have round morphology with relatively uniform size-distribution. There is no significant morphological difference among MBs, EPI-MBs and EPI-MBs+mAb. Figure 1(B) indicates the images of EPI-MBs+Ab with green fluorescence, EPI-MBs+Ab with red fluorescence and merged morphous of EPI-MBs+Ab observed under a confocal laser scanning microscope, which proved successful loading of EPI and conjugation of FITC-streptavidin. The average grain diameter and zeta potential in the EPI-MBs are 461.3 ± 50.2 nm and -16.6 ± 2.23 mV (Figure 1C and D). They are 483.8 ± 63.5 nm and -18.1 ± 4.07 mV in EPI-MBs+mAb (Figure 1E and F). The drug encapsulation efficiency of EPI-MBs and EPI-MBs+mAb is $71.9 \pm 2.3\%$ and $65.2 \pm 6.1\%$. The *in vitro* stability of C_3F_8 MBs experiments shows that the C_3F_8 can be kept in MBs for about one week.

Identification of CD138$^-$CD34$^-$CSCs in human RPMI 8226 cell line

According to the previous studies by others [9] and by us [27,28], CD138$^-$CD34$^-$ cells were presumed as CSCs in MM

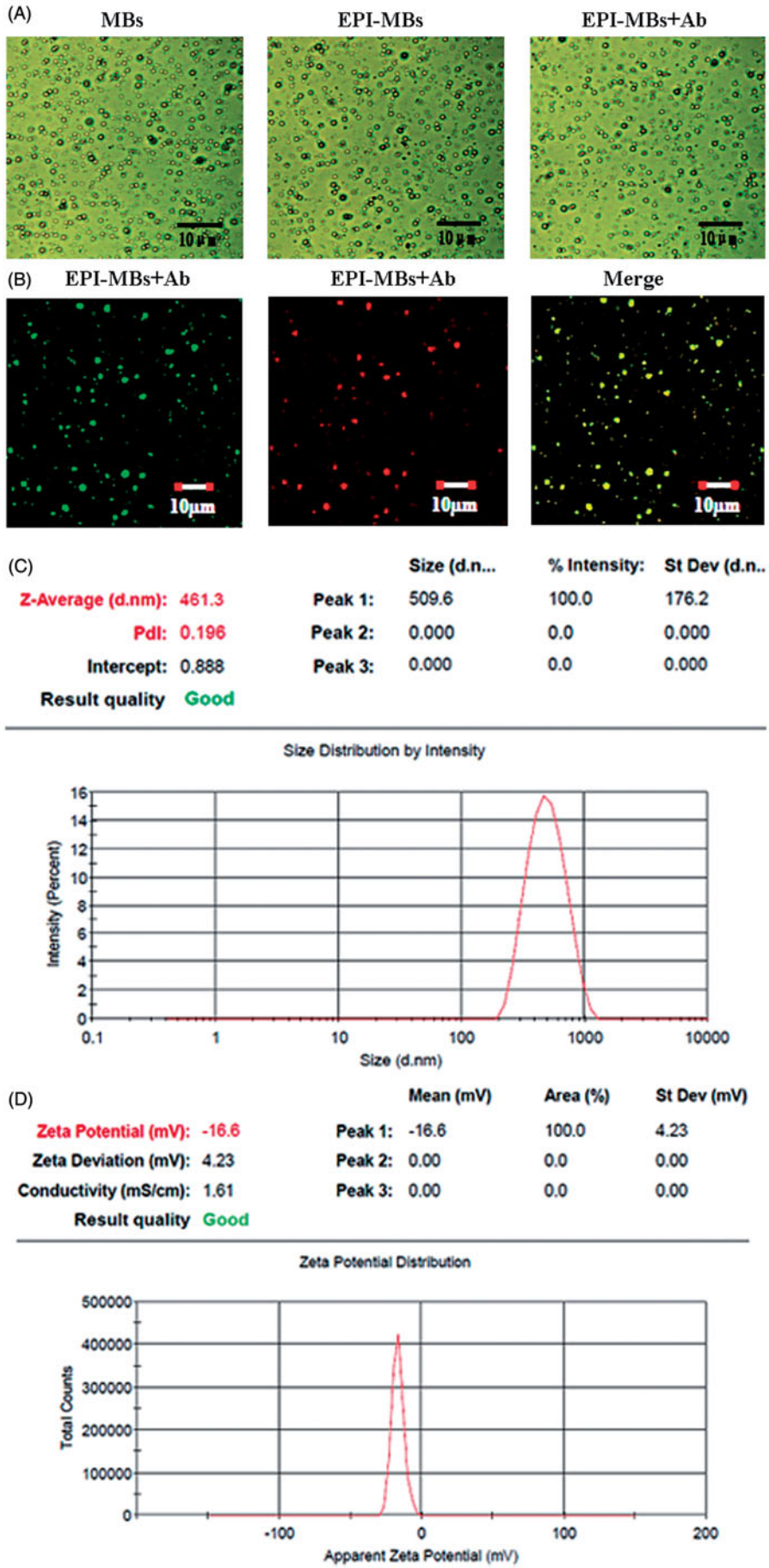

Figure 1. Images, size distribution and the zeta potential of MBs, EPI-MBs and EPI-MBs+mAb. (A) Optical microscopy images of MBs, EPI-MBs and EPI-MBs+mAb (400×). (B) Laser scanning confocal microscope images of EPI-MBs+mAb (dark field, 1000×). (C, D) The size distribution of EPI-MBs and the zeta potential of EPI-MBs. (E, F). The size distribution of EPI-MBs+mAb and the zeta potential of EPI-MBs+mAb.

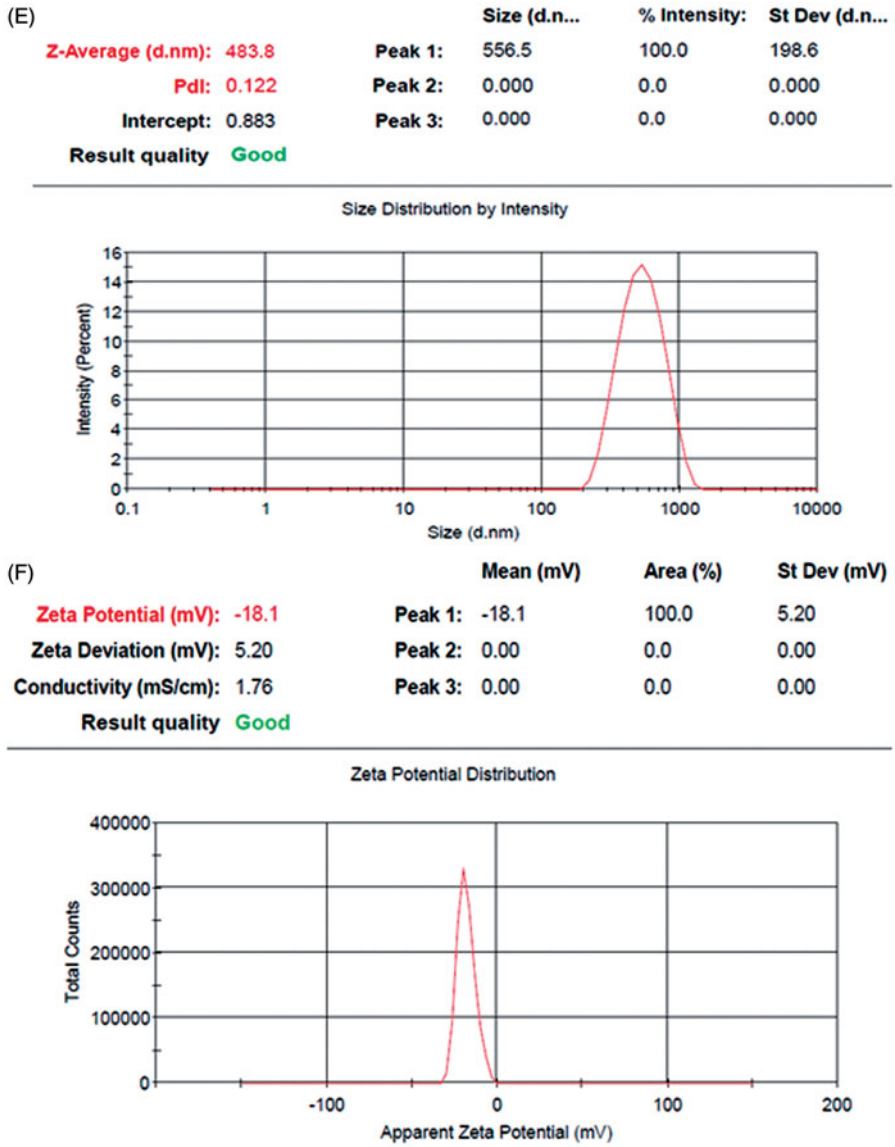

Figure 1. Continued.

RPMI 8226 cell line. Therefore, we first isolated $CD138^-CD34^-$ cells from the RPMI 8226 cell line, and then the ability of cell proliferation, clone formation, drug resistance, migration and invasion was characterized, respectively in our current study. The results from Figure 2(A–C) show that $CD138^-CD34^-$ cells had a significant higher proliferation potential after 6-day culture ($21\,666 \pm 2081$ cells versus $13\,666 \pm 1527$ cells, $p < 0.01$), and exhibited markedly stronger clone formation ability after 14-day culture ($26.67\% \pm 6.50\%$ versus $9.33\% \pm 3.21\%$, $p < 0.05$) than non-$CD138^-CD34^-$ cells. $CD138^-CD34^-$ cells also exhibited greater migration and invasion activity ($72.07\% \pm 4.78\%$ and $50.60\% \pm 2.57\%$, respectively) than non-$CD138^-CD34^-$ cells, while those of non-$CD138^-CD34^-$ cells were only $39.28\% \pm 5.34\%$ and $32.08\% \pm 3.65\%$, and the differences were a statistically significant ($p < 0.01$) as is shown in Figure 2(D and E). After 48 h of exposure to 10 μg/ml of EPI, $CD138^-CD34^-$ cells showed a significant lower inhibitor rate ($23.73\% \pm 6.17\%$) than non-$CD138^-CD34^-$ cells ($54.32\% \pm 4.61\%$) as is shown in Figure 2(F) ($p < 0.01$). In order to confirm the high expression of ABCG2 in RPMI 8226 cell line, $CD138^-CD34^-$ cells and non-$CD138^-CD34^-$ cells were isolated and analyzed by Western blot. Figure 2(G) exhibits that the ABCG2 band in $CD138^-CD34^-$ cells was stronger than that in non-$CD138^-CD34^-$ cells. These results suggest that $CD138^-CD34^-$ cells in RPMI 8226 cells possess the characteristics of CSCs that have the potential to give rise to tumor cell propagation through their self-renewal.

Surface binding of mAb and EPI accumulation in MM CSCs

EPI-MBs+mAb were synthesized by conjugating EPI-MBs with anti-ABCG2 mAb by a biotin–streptavidin–biotin linkage. FITC-labeled goat anti-mouse IgG was, respectively, added to the biotinylated MBs and the EPI-MBs+Ab. After incubation and wash, the EPI-MBs+Ab appeared bright green fluorescence (left) under a confocal laser scanning microscope, but no green fluorescence was observed on the biotinylated EPI-MBs (right) in Figure 3(A). This suggests that anti-ABCG2 mAb was successfully bound on the surface

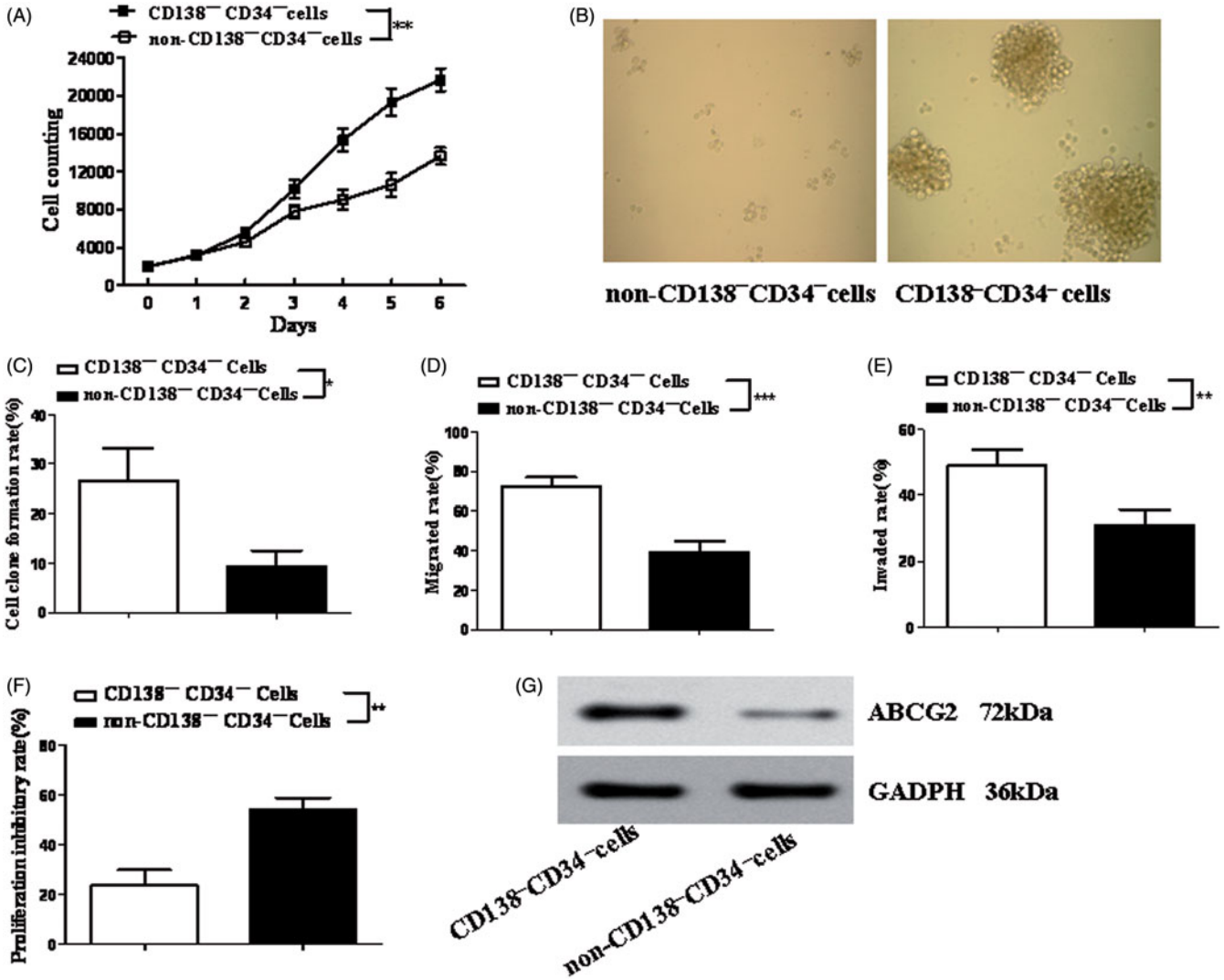

Figure 2. Analysis of CD138⁻CD34⁻ cell properties. (A) Cellular proliferation ability. (B) Clonal formation ability. (C) Clonal formation rate. (D) Cell migratory rate. (E) Cell invasive rate. (F) Proliferation inhibition rate when the cells were incubated with EPI for 48 h. (G) ABCG2 molecular expression analyzed by Western blot. $*p<0.05$, $**p<0.01$ and $***p<0.001$ were calculated by Student–Newman–Keuls.

of the EPI-MBs+Ab and still kept the immunobiologic activity. Because of high expression of ABCG2 molecule on the surface of MM CSCs, the EPI-MBs+mAb were prepared to block the chemotherapeutic drug EPI efflux from MM CSCs mediated by ABCG2 molecular pump. Figure 3(B) indicates the images of the MB binding of MM CSCs observed under a confocal laser scanning microscope after EPI-MBs+Ab (left) or EPI-MBs (right) were cultured with MM CSCs, which suggested that the EPI-MBs+Ab bound the cells well, whereas EPI-MBs did not bind on any cells. Figure 3(C) shows the fluorescence intensity of EPI-MBs and EPI-MBs+mAb after incubation with FITC-conjugated secondary antibody. The EPI-MBs+mAb show significant shift of the fluorescence count peak, indicating the high ABCG2 mAb binding affinity. In comparison, EPI-MBs show nearly no shift. There is a significant difference between the conjugation efficiency of the EPI-MBs+mAb group (130.38 ± 4.57) and the control group (4.73 ± 0.69, $p<0.001$) or the EPI-MB group (6.85 ± 1.02, $p<0.001$). Figure 3(D–E) gives that EPI accumulation in MM CSCs was significantly increased in the EPI-MBs+US group (231.29 ± 17.16) compared with the EPI group (35.24 ± 6.01, $p<0.01$) or the EPI+US group (29.16 ± 5.76, $p<0.01$). The further enhancement of EPI retention was remarkably elevated in the EPI-MBs+mAb+US group (276.16 ± 2.05) in contrast with the EPI-MBs+US group ($p<0.05$) or the EPI group ($p<0.001$) as are shown in Figure 3(D) and (E). The results demonstrated that the combination of the EPI-MBs+mAb bound to MM CSCs with ultrasound exposure could effectively target MM CSCs and accompany more EPI accumulation in MM CSCs.

Effect of ultrasound on MM CSCs

To analyze the effect of ultrasound on MM CSCs, we observed the cellular apoptosis and the cellular ultrastructural changes when the cells were alone exposed to ultrasound. Figure 4(B–D) indicates that compared with the control group, exposure to ultrasound ($0.5\,W/cm^2$, 40 s) neither induced MM CSC apoptosis nor inhibited the proliferation of MM CSCs, and that no ultrastructural changes were found in MM CSCs, suggesting that ultrasound itself has no obvious inhibitory effect on MM CSCs. The ultrasound exposure system is shown in Figure 4(E).

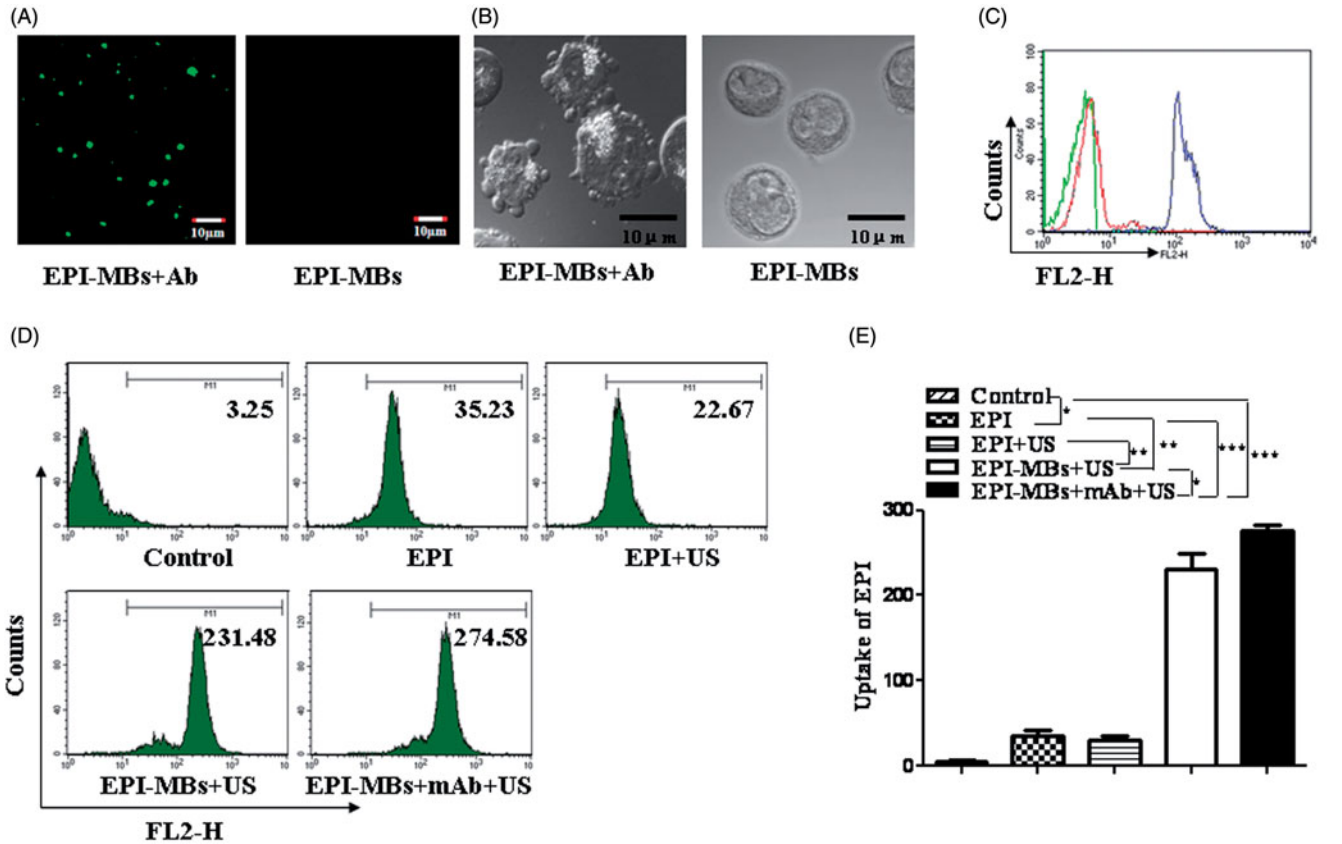

Figure 3. Anti-ABCG2 mAb targeted bind to MM CSCs and uptake of EPI by cells incubated with a various agents. (A) After adding FITC-labeled secondary antibody to the EPI-MBs+mAb, the surface of the MBs exhibited green fluorescence under a laser scanning confocal microscope (left, 1000×), but the EPI-MBs exhibited no fluorescence (right, 1000×). (B) EPI-MBs+mAb bound to MM CSCs (left), and no EPI-MBs bound to MM CSCs (right), which were observed under a laser scanning confocal microscope, 1000×. (C) Fluorescent intensity acquired by flow cytometry for EPI-MBs and EPI-MBs+mAb after incubation with FITC labeled secondary antibody. Green: Control (4.73 ± 0.69). Red: EPI-MBs (6.85 ± 1.02). Blue: EPI-MBs+mAb (130.38 ± 4.57). (D) EPI accumulation in MM CSCs incubated with the various agents and ultrasound exposure. (E) Analysis of EPI uptake by MM CSCs incubated with the various agents. $^{*}p < 0.05$, $^{**}p < 0.01$ and $^{***}p < 0.001$ were calculated by Student-Newman-Keuls with Bonferroni correction if multiple comparisons were involved, referring to the difference as compared to the normal group.

Cell viability after incubated with a various agents combined with ultrasound exposure

To evaluate the impact of UTMD on MM CSCs treated with the different chemotherapeutic agents, we used a CCK8 assay for this investigation. Figure 5 shows that the inhibitory rate on MM CSCs was a quite different after cells were incubated with the different agents in 24, 48 and 72 h. The inhibitory rate of cell proliferation in the EPI+US ($22.84\% \pm 3.94\%$), EPI-MBs+US ($39.18\% \pm 5.74\%$) and EPI-MBs+mAb+US ($54.02\% \pm 6.51\%$) groups was higher than that in the EPI ($17.51\% \pm 2.37\%$), EPI-MBs ($5.53\% \pm 2.29\%$) and EPI-MBs+mAb ($6.94\% \pm 2.02\%$) groups, respectively in 24 h. The differences were statistically significant ($p < 0.05$ or $p < 0.01$ or $p < 0.001$), in which the inhibitory rate in the EPI-MBs+mAb+US group was the highest among all groups. However, the difference between the EPI group and the EPI+US group was not statistically significant ($p > 0.05$). In 48 and 72 h, the similar results as in 24 h are found in Figure 5. The data suggested that UTMD of EPI-MBs significantly inhibited the cell proliferation, whereas the drug EPI was almost retained in the MBs without using UTMD.

Inhibition of MM CSC migration and invasion ability and increase of apoptosis

Figure 6(A and C) indicates that the migration and invasion rate of MM CSCs were significantly decreased in the EPI-MBs+mAb+US group ($25.52 \pm 4.49\%$ and $13.75 \pm 2.40\%$) compared with the EPI-MBs+mAb ($69.47 \pm 8.27\%$ and $51.29 \pm 8.01\%$, $p < 0.001$), EPI-MBs ($71.80 \pm 8.69\%$ and $52.61 \pm 8.01\%$, $p < 0.001$), EPI-MBs+US ($43.34 \pm 5.12\%$ and $30.32 \pm 4.52\%$, $p < 0.01$), the EPI group ($54.79 \pm 8.23\%$ and $42.05 \pm 9.06\%$, $p < 0.001$) and the PBS group ($73.07 \pm 4.92\%$ and $50.60 \pm 4.87\%$, $p < 0.001$), respectively 24 h after the MM CSCs were incubated with a various agents. The statistical analysis is shown in Figure 6(B and D).

The quantitative analysis by FCM showed that the apoptosis of MM CSCs was markedly increased 24 h after cells were incubated with the different agents. It was found in Figure 7 that the apoptosis rate was around $3.0 \pm 0.79\%$, $13.89 \pm 3.20\%$, $12.07 \pm 1.07\%$, $4.02 \pm 1.01\%$, $24.24 \pm 2.11\%$, $3.40 \pm 0.20\%$ and $38.35 \pm 4.05\%$ in the control, EPI, EPI+US, EPI-MBs, EPI-MBs+US, EPI-MBs+mAb and EPI-MBs+mAb+US groups in order. In comparison with the other treated groups, the EPI-MBs+mAb+US group resulted

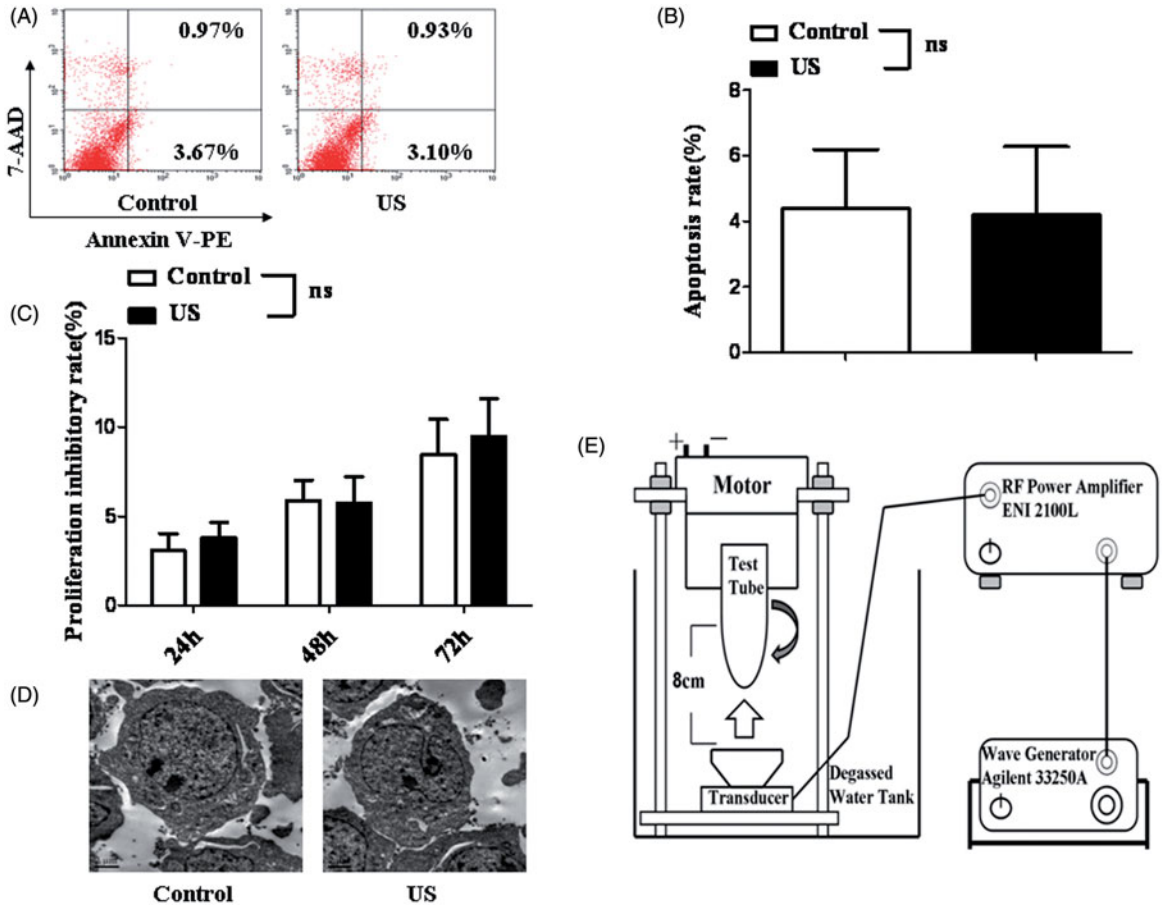

Figure 4. Observation of the apoptosis, the proliferative inhibitory rate and the ultrastructural changes of MM CSCs after ultrasound exposure. (A) MM CSC apoptosis was analyzed by FCM. (B) Quantification of apoptotic MM CSCs. (C) Cellular proliferative inhibitory rate was determined by Cell Counting Kit. (D) Ultrastructural images of MM CSCs. (E) The ultrasound exposure system. $*p<0.05$, $**p<0.01$ and $***p<0.001$.

in a significantly increased apoptosis rate, suggesting the increase of apoptosis was induced by anti-ABCG2 mAb targeting MM CSCs combined with ultrasound-mediated delivery of EPI from the MBs.

It was also found that the apoptosis rate in the EPI-MBs+US group was higher than any other groups except the EPI-MBs+mAb+US group, indicating EPI release and increase of cell membrane permeabilization after ultrasound action. There was no statistically significant difference ($p>0.05$) between the apoptosis rate of the EPI group ($13.89\pm3.20\%$) and the EPI+US group ($12.07\pm1.07\%$), suggesting the ultrasound itself did no harm to MM CSCs. In addition, the similar apoptosis among the control, EPI-MBs, EPI-MBs+mAb groups implies that the EPI-MBs and EPI-MBs+mAb did hardly mediate the EPI delivery in 24 h due to without ultrasound exposure.

Cellular morphology and caspase expression changes in MM CSCs

Figure 8(A) shows representative TEM images of MM CSC ultrastructural changes examined by TEM in a separate group 24 h after cells were incubated with the different agents. MM CSC ultrastructural changes indicated the cellular membrane damage, chromatin condensation and margination differently, especially in the EPI-MBs+mAb+US group, where cells exhibited obvious apoptotic characteristics. However, the morphological characteristics of MM CSCs incubated with EPI-MBs were almost the same as one of MM CSCs incubated with EPI-MBs+mAb.

In addition, the caspase expression changes were detected by Western blot assay. Figure 8(B) shows the expression changes of caspase-9, caspase-8 and caspase-3 in MM CSCs incubated with the different agents. The result from caspase-9 expression showed that the activity of caspase-9 was significantly increased in cells incubated with the EPI, EPI-MBs+US and EPI-MBs+mAb+US, respectively, compared with that of the PBS control cells, of which the caspase-9 activity in the EPI-MBs+mAb+US group was the highest among all groups, and it was reflected in high cleaved caspase-9 expression. The result from caspase-3 expression indicated a similar one as did caspase-9 expression. However, caspase-8 activity was not increased dramatically. Statistical analysis of caspase expressive changes in MM CSCs is shown in Figure 8(C).

Discussion

Increasing evidence has demonstrated that MM is initiated by CSCs and cure of MM needs to root out CSCs. To this regard, we first isolated $CD138^{-}CD34^{-}$ cells from human MM RPMI 8226 cell line and identified the cell traits, which showed MM CSC's characteristics as determined by a series of *in vitro* assays, indicating a stronger self-renewal, colony

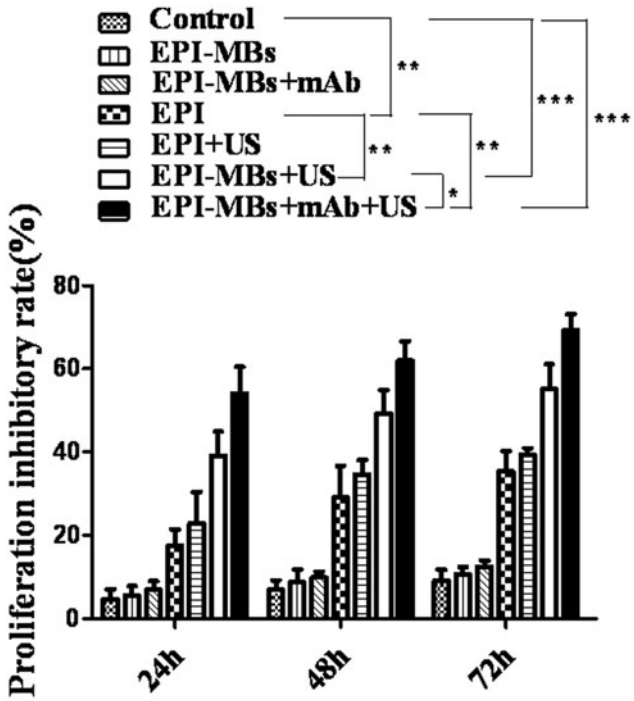

Figure 5. Proliferative inhibitory rate of MM CSCs incubated with a various agents. (A) Cellular proliferative inhibitory rate was determined by Cell Counting Kit on 24, 48 and 72 h after MM CSCs were incubated with the various agents. $*p<0.05$, $**p<0.01$ and $***p<0.001$, referring to the differences as indicated.

formation, migratory and invasive ability, and a higher ABCG2 expression than those of non-$CD138^{-}CD34^{-}$ cells [27–29]. To effectively target treatment of MM CSCs and reduce agent's side effects, we next developed EPI-loaded MBs with conjugated anti-ABCG2 mAb for allowing MBs to accumulate at MM CSCs and release EPI for a long time. In order to increase the efficacy of mAb binding to MBs, EPI-MBs+mAb were synthesized by conjugating a modified anti-ABCG2 mAb to the MBs of EPI-MBs *via* avidin−biotin interaction, which resulted in high mAb binding efficacy and good dispersity of EPI-MBs+mAb. In addition, the EPI-MBs+mAb were able to achieve 65% of drug encapsulation efficiency.

The data from this study show that the EPI-MBs+mAb+US exhibited more obvious inhibitory effect on MM CSC's proliferation, migration and invasion ability, and increase of cell cycle arrest and apoptosis than did any other agents. Although the EPI-MBs+mAb also exhibited a good inhibitory effect on MM CSCs this effect was not so strong as the EPI-MBs+US did. This is because there was no use of UTMD technique so as to not release EPI from MBs in spite of the use of anti-ABCG2 mAb that could directly target the ABCG2 molecule expressed highly on the surface of MM CSCs. FCM analyses showed that the increased accumulation of EPI in MM CSCs mediated by the EPI-MBs+US, and that the EPI-MBs+mAb led to more EPI accumulation in MM CSCs after ultrasound exposure. Accordingly, the EPI-

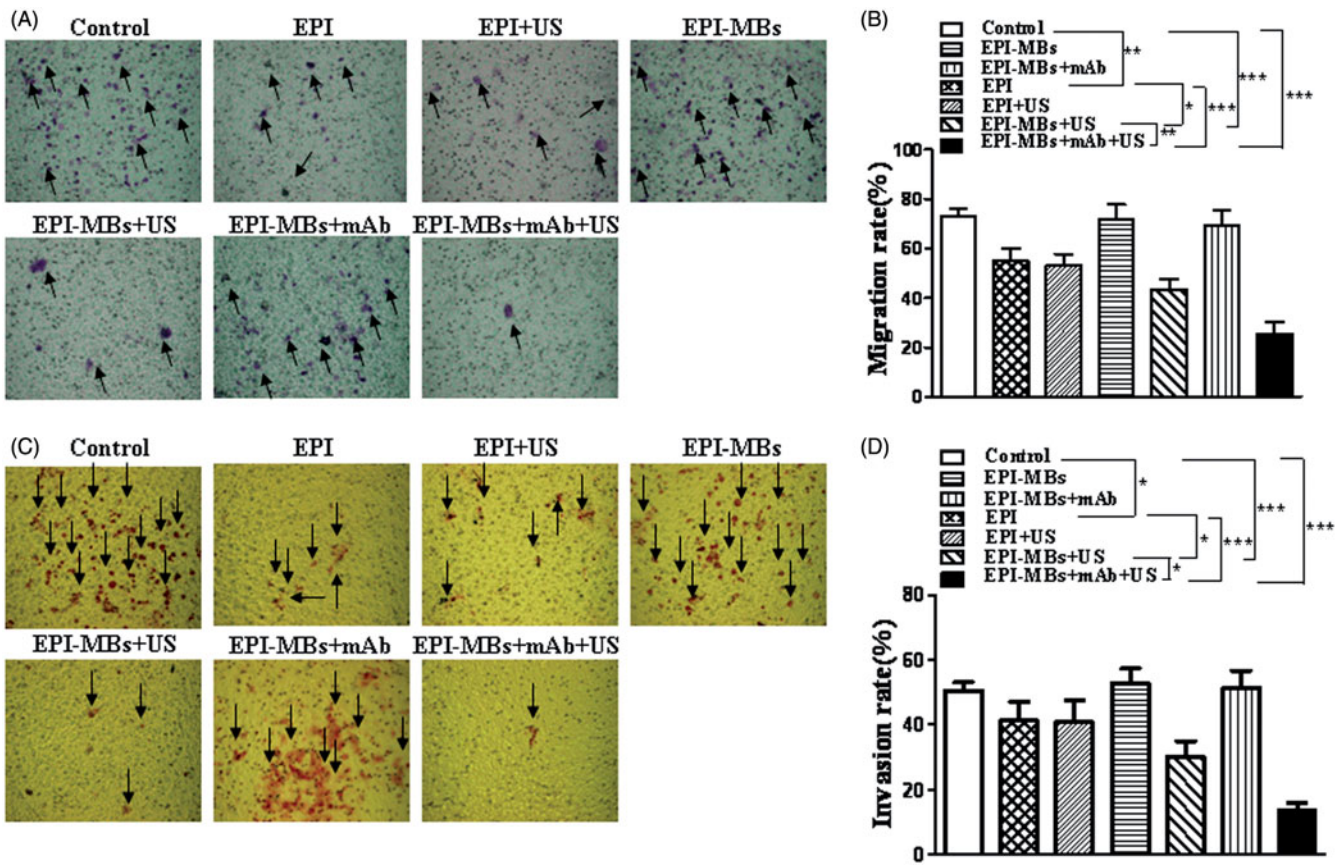

Figure 6. Observation of the migration and invasion ability of MM CSCs incubated with a various agents. Migration (A) and invasion (C) rates of MM CSCs were determined by transwell assay. (B) and (D) indicate the statistical analysis. Data are represented as mean ± SD. The assays were repeated for three times. $*p<0.05$, $**p<0.01$ and $***p<0.001$, referring to the differences as indicated.

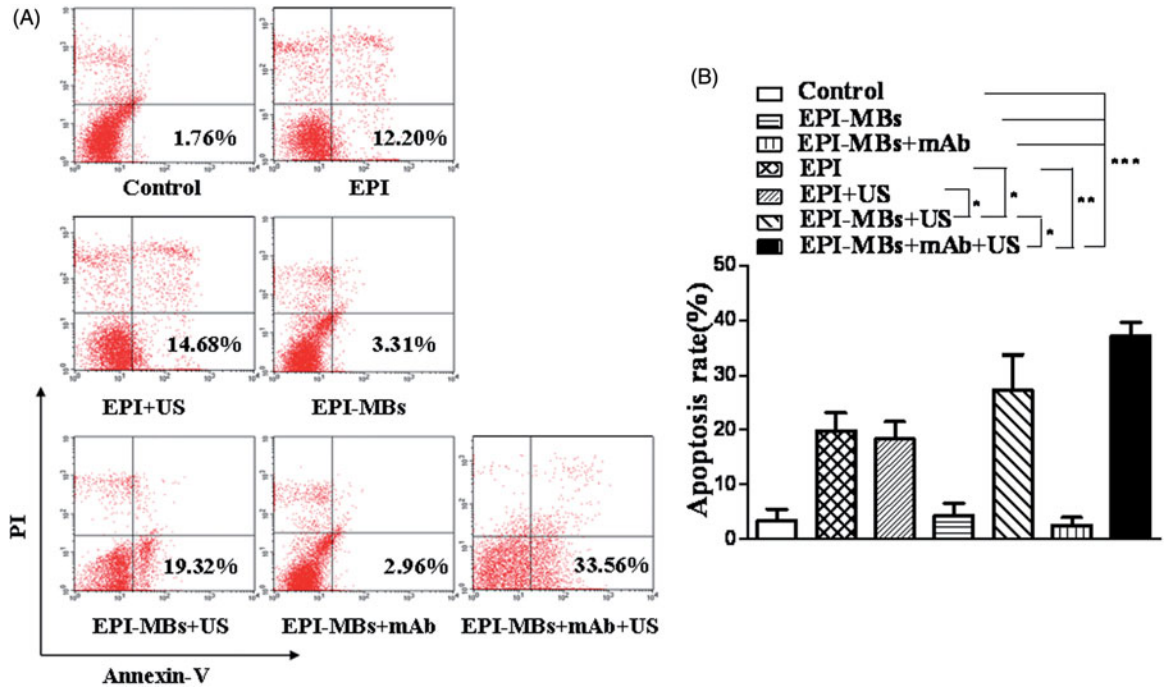

Figure 7. Analysis of MM CSC apoptosis treated with a various agents. (A) MM CSC apoptosis was analyzed by FCM after cells were treated with a various agents 24 h. (B) Quantification of apoptotic MM CSCs. $^{*}p<0.05$, $^{**}p<0.01$ and $^{***}p<0.001$.

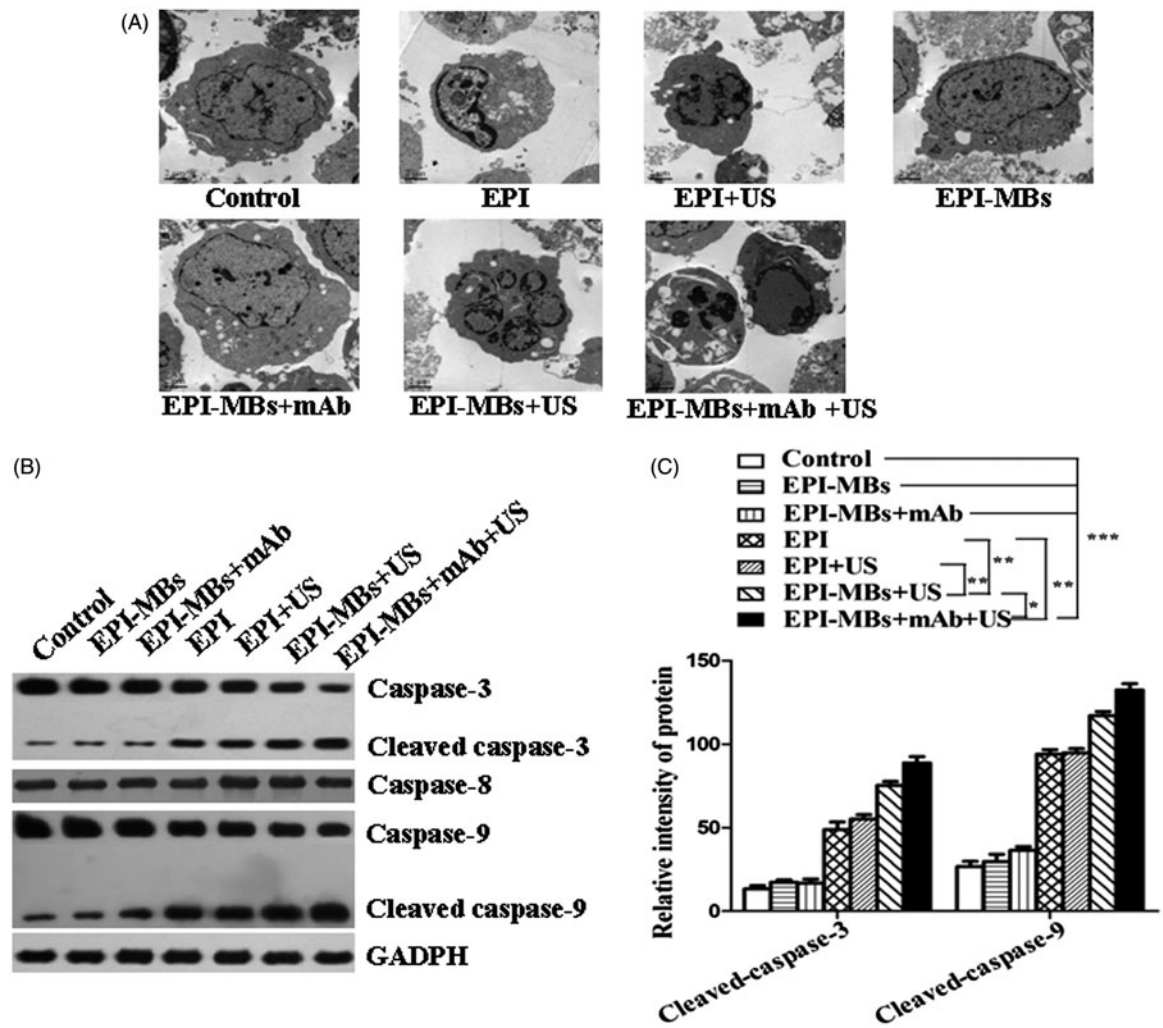

Figure 8. Ultrastructural characteristics and caspase expression of MM CSCs. (A) Ultrastructural images of MM CSCs observed under a TEM 24 h after cells were treated with the various agents. (B) Caspase expression analyzed by Western blot. (C) Relative intensity of caspase expression. Scale bar is 2 μm.

MBs+mAb+US markedly induced the MM CSC apoptosis and the cell morphology revealed an obvious apoptotic characteristics. In addition, Western blot analyses further confirmed that the apoptosis of MM CSCs was mediated by the activation of caspase-9 and caspase-3 *via* death receptor-mediated external signals or *via* mitochondria-mediated internal signals [39–41].

We guess that the mechanisms of UTMD function in this study may involve in (1) therapeutic ultrasound destroys the MBs and releases EPI from the MBs to the site of MM CSCs, which can promote EPI to easily enter cells through perforations in the membrane while ultrasound itself is not associated to any appreciable interference with MM CSC growth; (2) the MBs with conjugated anti-ABCG2 mAb were bound to the ABCG2 molecule on the surface of MM CSCs, which can make more MBs gathering around MM CSCs and cause more local EPI release from the MBs under ultrasound action; (3) anti-ABCG2 mAb can block the ABCG2's pump function and keep the EPI in the cells for developing cytotoxic effect on MM CSCs. These results suggest that the synergetic induction of inhibitory efficacy depends on combination of the EPI-MBs+mAb with UTMD technique. In our current study, we understand that it would be better to evaluate whether this anti-MM CSC regimen could lead to reduction of MM $CD138^-CD34^-$CSC growth in MM-bearing mice.

In summary, the data presented here revealed a novel aspect on the inhibition of MM $CD138^-CD34^-$CSC amplification by blocking the EPI efflux from the MM CSCs mediated by anti-ABCG2 mAb and resulting in MM CSC apoptosis *in vitro*. This preliminary study represents the first attempt to demonstrate that the mAb-conjugated MBs-based EPI-delivery vehicle may be regarded as a promising nano-device to deliver anti-MM drug EPI under ultrasound exposure, and as a potential anti-MM component in an effort to improve MM treatment outcome and reduce chemotherapeutic side effects.

Declaration of interest

The authors declare no conflict of interest.

The study has been supported by the 973 National Nature Science Foundation of People's Republic of China (2011CB933500), and supported by the Fundamental Research Funds for the Central Universities, Southeast University (3290005416).

References

1. Borrello I. Can we change the disease biology of multiple myeloma? Leuk Res 2012;36:S3–S12.
2. Bladé J, Cibeira MT, Fernández de Larrea C, et al. Multiple myeloma. Ann Oncol 2010;21: vii313–19.
3. Saini N, Mahindra A. Therapeutic strategies for the treatment of multiple myeloma. Discov Med 2013;15:251–8.
4. Chou T. Multiple myeloma: recent progress in diagnosis and treatment. J Clin Exp Hematopathol 2012;52:149–59.
5. Paíno T, Ocio EM, Paiva B, et al. CD20 positive cells are undetectable in the majority of multiple myeloma cell lines and are not associated with a cancer stem cell phenotype. Haematologica 2012;97:1110–14.
6. Agarwal JR, Matsui W. Multiple myeloma: a paradigm for translation of the cancer stem cell hypothesis. Anti-Cancer Agents Med Chem 2010;10:116–20.
7. Ghosh N, Matsui W. Cancer stem cells in multiple myeloma. Cancer Lett 2009;277:1–7.
8. Fratino L, Rupolo M, Mazzuccato M, et al. Autologous stem cell transplantation and multiple myeloma cancer stem cells. Anticancer Agents Med Chem 2013;13:1419–29.
9. Matsui W, Huff CA, Wang Q, et al. Characterization of clonogenic multiple myeloma cells. Blood 2004;103:2332–6.
10. Hajek R, Okubote SA, Svachova H. Myeloma stem cell concepts, heterogeneity and plasticity of multiple myeloma. Br J Haematol 2013;163:551–64.
11. Villa R, Cerroni B, Viganò L, et al. Targeted doxorubicin delivery by chitosan-galactosylated modified polymer microbubbles to hepatocarcinoma cells. Colloids Surf B Biointerfaces 2013;110: 434–42.
12. Geers B, De Wever O, Demeester J, et al. Targeted liposome-loaded microbubbles for cell-specific ultrasound-triggered drug delivery. Small 2013;9:4027–35.
13. Ren ST, Liao YR, Kang XN, et al. The antitumor effect of a new docetaxel-loaded microbubble combined with low-frequency ultrasound in vitro: preparation and parameter analysis. Pharm Res 2013;30:1574–85.
14. Sorace AG, Warram JM, Umphrey H, et al. Microbubble-mediated ultrasonic techniques for improved chemotherapeutic delivery in cancer. J Drug Target 2012;20:43–54.
15. Azmin M, Harfield C, Ahmad Z, et al. How do microbubbles and ultrasound interact? Basic physical, dynamic and engineering principles. Curr Pharm Des 2012;18:2118–34.
16. Wang Y, Bai WK, Shen E, et al. Sonoporation by low-frequency and low-power ultrasound enhances chemotherapeutic efficacy in prostate cancer cells in vitro. Oncol Lett 2013;6:495–8.
17. Liu H, Chang S, Sun J, et al. Ultrasound-mediated destruction of LHRHa-targeted and paclitaxel-loaded lipid microbubbles induces proliferation inhibition and apoptosis in ovarian cancer cells. Mol Pharm 2014;11:40–8.
18. Abe M, Harada T, Matsumoto T. Concise review: defining and targeting myeloma stem cell-like cells. Stem Cells 2014;32: 1067–73.
19. Lu CT, Zhao YZ, Wu Y, et al. Experiment on enhancing antitumor effect of intravenousepirubicin hydrochloride by acoustic cavitation in situ combined with phospholipid-based microbubbles. Cancer Chemother Pharmacol 2011;68:343–8.
20. Tinkov S, Coester C, Serba S, et al. New doxorubicin-loaded phospholipid microbubbles for targeted tumor therapy: in vivo characterization. J Control Release 2010;148:368–72.
21. Tinkov S, Winter G, Coester C, Bekeredjian R. New doxorubicin-loaded phospholipid microbubbles for targeted tumor therapy: Part I – formulation development and in vitro characterization. J Control Release 2010;143:143–50.
22. Yang F, Zhang M, He W, et al. Controlled release of Fe_3O_4 nanoparticles in encapsulated microbubbles to tumor cells via sonoporation and associated cellular bioeffects. Small 2011;7: 902–10.
23. Wang C, Yang F, Xu Z, et al. Intravenous release of NO from lipidic microbubbles accelerates deep vein thrombosis resolution in a rat model. Thromb Res 2013;131:e31–8.
24. Yang F, Gu N, Chen D, et al. Experimental study on cell self-sealing during sonoporation. J Control Release 2008;131: 205–10.
25. Wang L, Li L, Guo Y, et al. Construction and in vitro/in vivo targeting of PSMA-targeted nanoscale microbubbles in prostate cancer. Prostate 2013;73:1147–58.
26. Niu C, Wang Z, Lu G, et al. Doxorubicin loaded superparamagnetic PLGA-iron oxide multifunctional microbubbles for dual-mode US/MR imaging and therapy of metastasis in lymph nodes. Biomaterials 2013;34:2307–17.
27. Yang CP, Xiong F, Wang J, et al. Anti-ABCG2 monoclonal antibody in combination with paclitaxel nanoparticles against cancer stem-like cell activity in multiple myeloma. Nanomedicine 2014;9:45–60.
28. Yang CP, Wang J, Chen D, et al. Paclitaxel-Fe_3O_4 nanoparticles inhibits the growth of $CD138^-CD34^-$ tumor stem-like cells in multiple myeloma bearing mice. Int J Nanomed 2013;8:1439–49.
29. Dou J, Pan M, Wen P, et al. Isolation and identification of cancer stem like cells from murine melanoma cell lines. Cell Mol Immunol 2007;4:467–72.

30. Chen DY, Wang J, Zhang Y, et al. Effect of downregulated transcriptional repressor ZEB1 on the epithelial-mesenchymal transition of ovarian cancer cells. Int J Gynecol Cancer 2013;23: 1357–66.
31. Lo YL, Ho CT, Tsai FL. Inhibit multidrug resistance and induce apoptosis by using glycocholic acid and epirubicin. Eur J Pharm Sci 2008;35:52–67.
32. Lo Y-L. A potential daidzein derivative enhances cytotoxicity of epirubicin on human colon adenocarcinoma Caco-2 cells. Int J Mol Sci 2013;14:158–76.
33. Chen JS, Wang J, Zhang Y, et al. Analysis of ovarian cancer stem cell behavior and drug resistance in a three dimensional cell culture. J Biosci Bioeng 2014;118:214–22.
34. Zhang Y, Hu H, Song L, et al. Epirubicin-mediated expression of miR-302b is involved in osteosarcoma apoptosis and cell cycle regulation. Toxicol Lett 2013;222:1–9.
35. Sun WL, Chen J, Wang YP, et al. Autophagy protects breast cancer cells from epirubicin-induced apoptosis and facilitates epirubicin-resistance development. Autophagy 2011; 7:1035–44.
36. Villa CH, Dao T, Ahearn I, et al. Single walled carbon nanotubes deliver peptideantigen into dendritic cells and enhance IgG responses to tumor-associated antigens. ACS Nano 2011;5: 5300–11.
37. Cirstea D, Hideshima T, Rodig S, et al. Dual inhibition of akt/mammaliantarget of rapamycin pathway by nanoparticle albumin-bound–rapamycin and perifosine induces antitumor activity in multiple myeloma. Mol Cancer Ther 2010;9:963–75.
38. Hu W, Wang J, Dou J, et al. Augmenting therapy of ovarian cancer efficacy by secreting IL-21 human umbilical cordblood stem cells in nude mice. Cell Transplant 2011;20:669–80.
39. Yang CP, He XF, Chen JS, et al. $Fe^{3}O^{4}$ nanoparticle loaded paclitaxel induce multiple myeloma apoptosis by cell cycle arrest and increase cleavage of caspases in vitro. J Nanopart Res 2013;15: 1840.
40. Twomey C, McCarthy JV. Pathways of apoptosis and importance in development. J Cell Mol Med 2005;9:345–59.
41. Li P, Nijhawan D, Budihardjo I, et al. Cytochrome c and dATP-dependent formation of Apaf-1/caspase-9 complex initiates an apoptotic protease cascade. Cell 1997;91:479–89.